scientific reports

Check for updates

OPEN

Design and in vitro evaluation of novel tetrazole derivatives of dianisidine as anticancer agents targeting Bcl-2 apoptosis regulator

Wioletta Olejarz[1,4], Karol Sadowski[1,4], Piotr Roszkowski[2], Anna Bielenica[3], Maciej Wiśniewski[5,6], Marta Struga[3] & Daniel Szulczyk[3]✉

This study examines the synthesis and biological evaluation of novel tetrazole derivatives of 3,3′-dimethoxybenzidine as potential anticancer agents, focusing on their cytotoxic, apoptotic, and anti-inflammatory properties. Ten derivatives were synthesized using thioureas as precursors, characterized through spectroscopic methods, and assessed for their in silico toxicological profiles using the ADMET-AI and ProTox 3.0 platforms. In vitro cytotoxic activity was evaluated against four human cancer cell lines (HTB-140, A549, HeLa, SW620) and one normal cell line (HaCaT) using MTT and LDH assays. Mechanistic studies included apoptosis assessment via flow cytometry and interleukin-6 (IL-6) analysis using ELISA. The synthesized tetrazole derivatives demonstrated significant anticancer potential, exhibiting selective cytotoxicity against cancer cell lines, robust induction of apoptosis, and a notable reduction in IL-6 levels. Their favorable toxicity profiles, as observed in both in silico and in vitro evaluations, support their potential as promising candidates for further development. The tested compounds showed strong inhibitory activity against the apoptosis regulator Bcl-2, with binding affinities comparable to those of native ligands. Western blot analysis revealed a dramatic loss of Bcl-2 protein expression in selected cancer cells during exposure to compound 5. Additionally, this research highlights the innovative use of hazardous substrates in drug discovery, aligning with the principles of green chemistry. Future efforts should focus on optimizing the most active derivatives and conducting in vivo studies to confirm their therapeutic potential and safety.

Keywords Tetrazoles, Cytotoxicity, Anticancer, Toxicology, Apoptosis

There is a call for the continuous search for novel anticancer agents with improved therapeutic profiles. In recent years, there has been an increasing interest in the synthesis of anticancer molecules derived from unconventional and often hazardous substrates[1–3]. These substrates, which are typically associated with toxicity and environmental hazards, have demonstrated unexpected potential in generating compounds with potent anticancer activities. Synthetic chemistry and biotechnology advancements have unveiled a promising paradox: these dangerous substances can be transformed into valuable anticancer agents[4–7]. This innovative approach leverages the natural bioactivity of these substrates, enabling the development of molecules that can selectively target cancer cells while sparing normal tissues. Firstly, it offers a novel chemical space for drug discovery, expanding the inventory of potential anticancer compounds. Secondly, it provides an opportunity for the valorization of toxic compounds, aligning with principles of green chemistry and sustainability. Thirdly, the unique structural features of molecules derived from hazardous substrates often discuss distinct mechanisms of action, potentially overcoming resistance pathways that limit the effectiveness of traditional anticancer drugs.

Benzidine and its derivatives such as 3,3′-dimethylbenzidine (o-tolidine), 3,3′-dimethoxybenzidine (o-dianisidine), and dichlorobenzidine (Fig. 1) are the starting materials for the synthesis of azo dyes[8,9].

[1]Department of Biochemistry and Pharmacogenomics, Faculty of Pharmacy, Medical University of Warsaw, 02-097 Warsaw, Poland. [2]Faculty of Chemistry, University of Warsaw, Pasteura 1, 02-093 Warszawa, Poland. [3]Department of Biochemistry, Medical University of Warsaw, 02-097 Warsaw, Poland. [4]Centre for Preclinical Research, Medical University of Warsaw, 02-097 Warsaw, Poland. [5]Laboratory of Bioinformatics and Computational Genomics, Faculty of Mathematics and Information Science, Warsaw University of Technology, Warsaw, Poland. [6]Laboratory of Functional and Structural Genomics, Centre of New Technologies, University of Warsaw, Warsaw, Poland. ✉email: daniel.szulczyk@wum.edu.pl

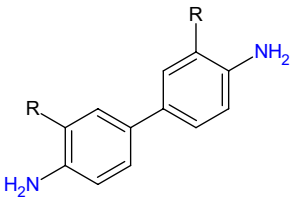

R= H [1,1'-biphenyl]-4,4'-diamine

R= -OCH_3 3,3'-dimethoxy[1,1'-biphenyl]-4,4'-diamine

R= -CH_3 3,3'-dimethyl[1,1'-biphenyl]-4,4'-diamine

R= -Cl 3,3'-dichloro[1,1'-biphenyl]-4,4'-diamine

Fig. 1. Structure and chemical names of popular azo dyes precursors.

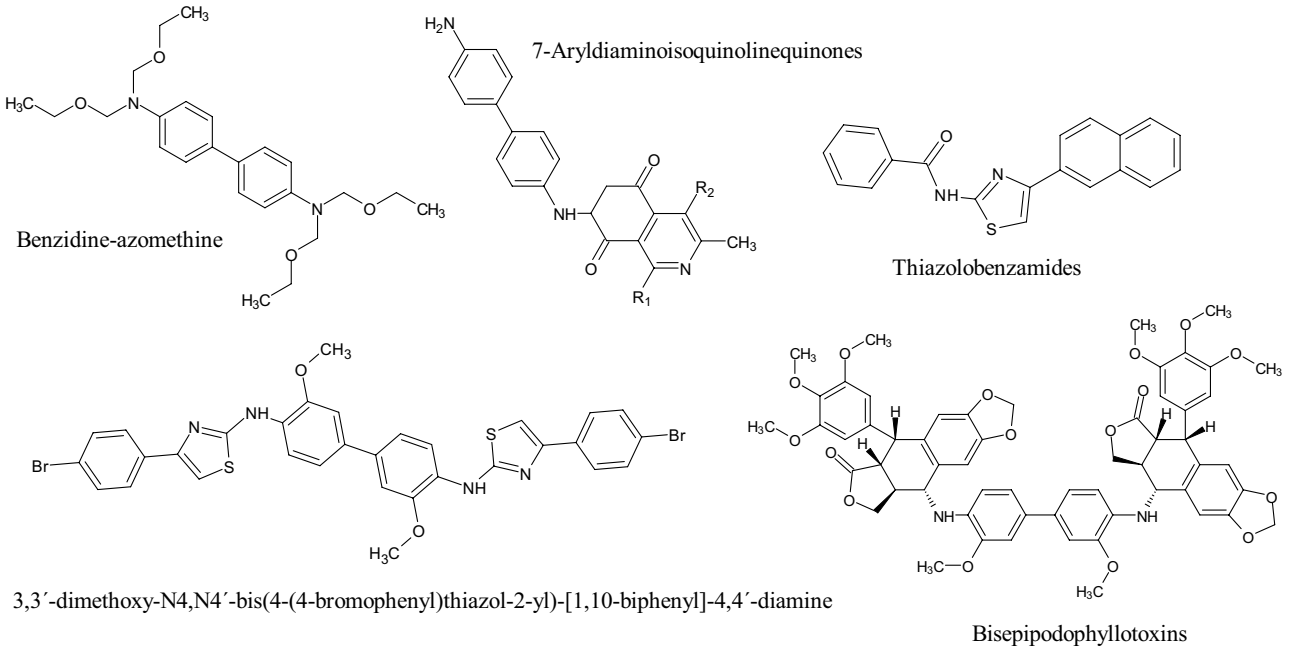

Fig. 2. Example benzidine-based structural motifs studied towards cancer cell lines.

National regulatory agencies monitor these azo dyers due to the possible carcinogenicity of incorporated amines[10]. Some scientists are searching for solutions to tackle the issue of detoxification of such compounds[11,12].

The simplest method to reduce toxicity and carcinogenic action is to modify the base structure responsible for such unfavorable properties. In benzidine studies, we can find examples of successful modifications leading to new derivatives possessing beneficial biological actions. In one of the publications, authors unveiled results on studied new benzidine-based azomethine derivates (Fig. 2). The anticancer properties of these were investigated against two cell lines (MDA-MB-231 human breast adenocarcinoma and DLD1 human colorectal adenocarcinoma cell lines) with a colorimetric assay using the tetrazolium salt WST-8. It was found that the benzidine-based azomethine derivatives had a significant anti-proliferative effect on the human breast cancer cell line (MDA-MB-231)[13]. Benzidine was also used as one of the starting materials in another study. The antiproliferative evaluation was performed on the series against normal mouse embryo fibroblast cell line MEF and three cancer cell lines: MDA-MB-21 human breast adenocarcinoma, B16-F10 murine metastatic melanoma, and CaCo-2 human intestinal carcinoma cells showed moderate to high potencies. The authors decided to plan further studies starting with synthesizing bivalent phenylaminoisoquinolinequinones (Fig. 2) using symmetrical aryldiamines connected through aliphatic spacers[14]. In a recent paper, authors claimed that a synthesized series of thiazolobenzamide molecules (Fig. 2) connected to naphthalene moiety inhibited the growth of three different tumor cell lines, MCF7 (breast carcinoma), A549 (pulmonary carcinoma), and DU145 (prostatic adenocarcinoma). Among these compounds, one was a dianisidine derivative. However, different leading compounds showed promising results against all cell lines, especially exceptional efficacy against breast cancer. Furthermore, when a dose of 50–500 mg/kg of the total mass of rats is given, this most effective compound did not exhibit any harmful effects during acute oral toxicity tests[15]. Eleven similar derivatives were studied in another work, but this time the most promising was derivative of dianisidine 3,3′-dimethoxy-N4,N4′-bis(4-(4-bromophenyl)thiazol-2-yl)-[1,10-biphenyl]-4,4′-diamine (Fig. 2) due to its notable inhibitory effects on A549 human lung adenocarcinoma, and C6 rat glioma cell lines and low toxicity to NIH/3T3 mouse embryonic fibroblast cell lines[16].

Four more complex compounds based on *o*-dianisidine core (Fig. 2) were studied and results were presented in the paper. These have been evaluated for their anticancer potential and DNA-topoisomerase II poisoning activity.

Most of the evaluated derivatives have exhibited promising in vitro anticancer activity against different human tumor cell lines and interestingly 4′-O-methylated analogs have shown increased cytotoxic activity. Similarly, the DNA-topo II poisoning activity tested for these compounds has not only exhibited the DNA cleavage potential comparable to etoposide, but for some compounds this cleavage potential was superior to etoposide[17]. Proteins from the Bcl-2 (B-2 cell lymphoma) family are key regulators of cell apoptosis, also involved in the processes of invasion and metastasis of cancer cells. The Bcl-2 protein group consists of pro-apoptotic inhibitors (BH3- only proteins) and effectors (like BAX, BAK proteins), as well as pro-survival guardians (represented by Bcl-2, Bcl-X proteins)[18,19]. The latter supports the viability of health cells by preventing the activation of BAX and BAK. In the case of various stress signals (e.g. cytokine or nutrient deficiencies, DNA damage, oncogenic factors), BH3-only proteins are increased in expression and bind pro-survival proteins, leading to apoptotic changes in the cell[18,20,21]. It has been shown that overexpression of Bcl-2 proteins in melanoma, lung, and colorectal cancer cells results in increased invasiveness of these cells[18,22–24]. Several Bcl-2 family members (Bcl-2, Bcl-X, Bcl-w, Mcl-1) promote cancer cell invasion and migration by inducing kinases (e.g. Src), transcription factors (e.g. AP-1), cell surface receptors (e.g. epidermal growth factor receptor—EGFR) or matrix-degrading enzymes (e.g. matrix metalloproteinase (MMP)-2)[22–25]. Moreover, Bcl proteins activate the production of mitochondrial reactive oxygen species (ROS) in leukemia, glioma, and lung cancer cells[25,26]. The generated ROS then influences various signaling pathways, increasing the risk of cancer metastasis. In addition, Bcl-2 protein inhibitors have recently been used in combination with aurora kinase suppressors in treating aggressive HPV + cervical cancers (Hela, CaSki cell lines)[27]. Most known Bcl-2 protein inhibitors are represented by complex polyphenyl derivatives[28], which include phenylpiperazine[29–32] or benzothiazole analogues[33,34]. The most common is polyaromatic Venetoclax, used in the treatment of chronic lymphocytic leukaemia and acute myeloid leukaemia, as well as in multidrug therapy of cervical cancer[27,29,30].

By utilizing all available tools such as in silico testing, molecular docking, novel synthetic methods, and comprehensive biological activity assays we can expand our research and explore new therapeutic approaches. Considering our team's past research experience[35–39] and the available data, we undertook studies on a new group of compounds based on the o-dianisidine core.

Our goal was to synthesize compounds with selective activity against cancer cell lines while minimizing cytotoxicity in normal cells and to elucidate their probable mechanism of action. We conducted several in vitro assays, including lactate dehydrogenase and interleukin-6 evaluations, on the most potent derivatives. Additionally, computer-aided techniques were applied. The obtained data contribute to the scientific community's understanding, particularly benefiting researchers developing new therapeutic strategies against cancer.

Results

Chemistry

We have designed a simple synthetic pathway to obtain novel tetrazole compounds using corresponding thioureas as substrates (Fig. 3). Such a transition is well-known and has been conducted many times by our team.

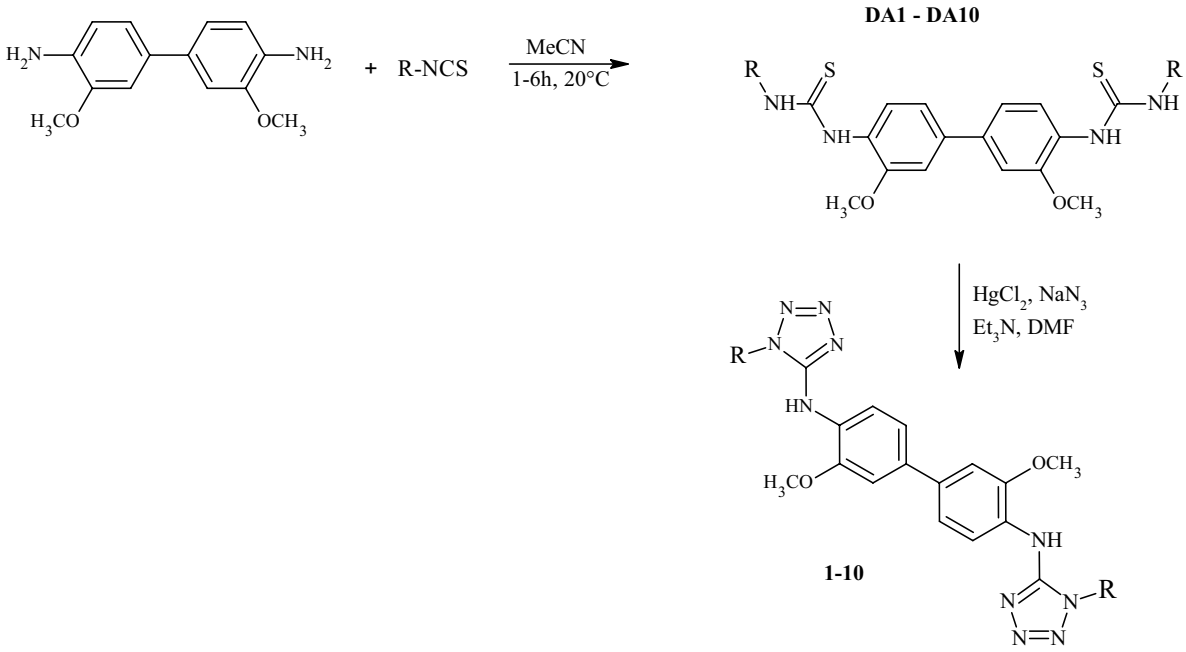

R: 3-chloro-4-fluorophenyl (**1**), 3-bromophenyl (**2**), 3-fluorophenyl (**3**), 3-chlorophenyl (**4**), 2-phenylethyl (**5**), 1-phenylethyl (**6**), benzyl (**7**), 4-iodophenyl (**8**), 3,4-dichlorophenyl (**9**), 3-trifluoromethylphenyl (**10**)

Fig. 3. Synthesis of novel 3,3′-dimethoxybenzidine tetrazoles.

Two (**DA9**–**DA10**) of the substrate thioureas were already synthesized and described by other researchers[40,41]. In this study, thioureas were synthesized solely as intermediates for the final tetrazoles and were not subjected to biological evaluation. However, spectral analysis of unpublished thiourea derivatives is provided in the supplementary file (see Supplementary Section S.2.1 Chemistry online). Tetrazoles were synthesized from their corresponding thiourea precursors using the procedure outlined in Sect. 3.1. For each product, spectrochemical characterization was provided (see Sects. 3.1.1–10 below). The NMR and MS spectra are available in the supplementary file (see Supplementary Figs. S.2–S.11 online).

In vitro cytotoxic activity

As an initial step in evaluating the cytotoxic properties of the derivatives, all tetrazoles were tested against four human carcinoma cell lines—HTB-140 (human melanoma), A549 (human lung adenocarcinoma), HeLa (cervical cancer), and SW620 (colorectal cancer) as well as the normal cell line HaCaT (immortalized human keratinocytes). Table 1 presents the half-maximal inhibitory concentration (IC_{50}, μM) values obtained using the MTT assay[42], comparing the tested compounds with two commonly used chemotherapeutic agents, cisplatin (**Ref 1**) and doxorubicin (**Ref 2**).

Some evaluated compounds (**3**, **4**, **5**, **7**, **8**, and **10**) showed moderate cytotoxic effects (Table 3). None of the investigated derivatives were selective against the A549 cell line, with concentration values ranging between 30 and 40 μM. Concluding, this cell line was less sensitive to the presence of the tested derivatives. However, five selectivity indexes exceeded a value of 1.5 for each of the three other cancer cell lines. Notably, for the HTB-140 cell line, the selectivity indexes of both reference products were higher than those of the active investigated drugs. In contrast, for the HeLa and SW620 cell lines, each derivative exhibited a higher selectivity index than the reference compounds, cisplatin and doxorubicin. The best selectivity was observed for compound **7** in the case of the HeLa cell line. Generally, the concentrations of the studied compounds were consistent across the cell lines, indicating that studies related to the influence of substituent changes on the core structure may not be necessary. Although superior results compared to the references were not found, derivatives **3** (R = 3-chlorophenyl), **4** (R = 3-fluorophenyl), and **7** (R = benzyl) demonstrated selectivity indexes above 1.5 for three cell lines. Consequently, we focused on these compounds from a group selected for further testing.

In silico toxicological properties

The rise of extensive chemical repositories and combinatorial chemical spaces, along with advancements in high-throughput docking and generative AI, has significantly broadened the chemical diversity of small molecules available for drug discovery. To choose compounds for experimental validation, it is essential to filter these molecules based on favorable drug-like properties, including Absorption, Distribution, Metabolism, Excretion, and Toxicity (ADMET). This paper examined target compounds using two prediction models for their toxicological and other physicochemical parameters. Firstly, a new ADMET-AI platform[43] was used to validate starting materials' use in synthesizing tetrazole derivatives of 3,3′-dimethoxybenzidine. The input derivatives were compared with predictions for 2579 approved drugs from the DrugBank database.

For the designed ten derivatives selected toxicity parameters were calculated and summarized in a table below (Table 2). For compound **1** visualization of selected toxicity parameters was demonstrated (Fig. 4).

No.	Cancer cells								Normal cells
	HTB-140[a]		A549[b]		HeLa[c]		SW620[d]		HaCaT[e]
	IC_{50}	SI	IC_{50}	SI	IC_{50}	SI	IC_{50}	SI	IC_{50}
1	**27.6 ± 6.7**	**1.54**	36.2 ± 6.3	1.17	41.5 ± 4.2	1.02	36.1 ± 5.4	1.18	42.6 ± 7.6
2	28.8 ± 3.2	1.43	36.5 ± 8.5	1.13	33.4 ± 3.9	1.23	37.2 ± 3.5	1.11	41.4 ± 8.5
3	**23.7 ± 4.7**	**1.91**	31.5 ± 9.1	1.43	**26.1 ± 4.9**	**1.73**	**27.6 ± 5.1**	**1.64**	45.3 ± 9.1
4	**22.2 ± 3.6**	**1.92**	35.3 ± 7.9	1.21	**24.4 ± 6.5**	**1.75**	**23.4 ± 6.6**	**1.82**	42.7 ± 7.9
5	33.7 ± 4.9	1.30	34.3 ± 8.3	1.27	**25.7 ± 3.7**	**1.70**	**24.5 ± 3.3**	**1.78**	43.8 ± 8.3
6	34.8 ± 3.9	1.22	36.3 ± 7.4	1.17	38.4 ± 4.9	1.11	33.4 ± 4.9	1.27	42.5 ± 6.4
7	**23.5 ± 4.1**	**1.71**	34.2 ± 6.3	1.17	**20.3 ± 3.8**	**1.98**	**21.3 ± 5.5**	**1.88**	40.2 ± 6.3
8	30.7 ± 2.6	1.30	35.4 ± 7.3	1.13	**25.4 ± 4.6**	**1.57**	31.7 ± 4.3	1.26	40.1 ± 7.3
9	32.3 ± 2.9	1.35	39.6 ± 7.6	1.10	35.5 ± 4.6	1.23	31.9 ± 4.3	1.37	43.6 ± 6.3
10	**27.9 ± 2.6**	**1.53**	33.6 ± 7.3	1.27	32.7 ± 4.6	1.30	**25.1 ± 4.3**	**1.70**	42.7 ± 7.3
Ref 1*	**1.4 ± 0.69**	**2.00**	2.7 ± 1.1	1.03	**1.8 ± 0.74**	**1.55**	1.9 ± 0.9	1.47	2.8 ± 1.1
Ref 2*	**0.5 ± 0.21**	**2.20**	0.9 ± 0.19	1.22	**0.6 ± 0.14**	**1.83**	**0.7 ± 0.16**	**1.57**	1.1 ± 0.19

Table 1. Cytotoxic activity (IC_{50}, μM) of tested compounds **1**–**10** determined by the MTT assay. Data are represented as IC_{50} (μM), i.e., the compound concentration corresponding to a 50% growth inhibition of a given cell line (compared to the control) after having cultured the cells for 72 h with the compound of interest. Three independent experiments were performed, each in triplicate. Data are expressed as mean ± SD. The SI (Selectivity Index) was calculated for each compound using a formula: SI = IC_{50} for normal cell line/IC_{50} cancer cell line. Compounds with SI greater or equal to 1.5 for both tumor cell lines have been bolded. *Ref 1 = cisplatin, **Ref 2—doxorubicin. [a]Human melanoma cell line. [b]Human lung adenocarcinoma cell line. [c]Cervical cancer cell line. [d]Colorectal cancer cell line. [e]Immortalized human keratinocytes.

Compound	Clinical toxicity	Mutagenicity	Carcinogenicity	Acute toxicity * LD_{50}
1	64.06	46.80	92.36	44.78
2	72.16	56.53	94.57	34.97
3	77.05	65.06	94.11	50.60
4	71.07	48.12	93.95	42.96
5	60.84	86.70	79.10	63.71
6	59.87	68.59	77.39	50.48
7	63.24	75.88	81.62	51.73
8	74.25	51.57	95.81	29.66
9	66.42	47.81	94.03	45.60
10	79.33	64.91	93.99	75.07
Ref 1**	89.92	99.03	10.62	83.52
Ref 2**	28.93	86.86	94.15	39.86

Table 2. Summary of toxicity evaluation expressed by DrugBank percentile (%). *log(1/(mol/kg)). **Ref 1 = doxorubicin, Ref 2 = cisplatin.

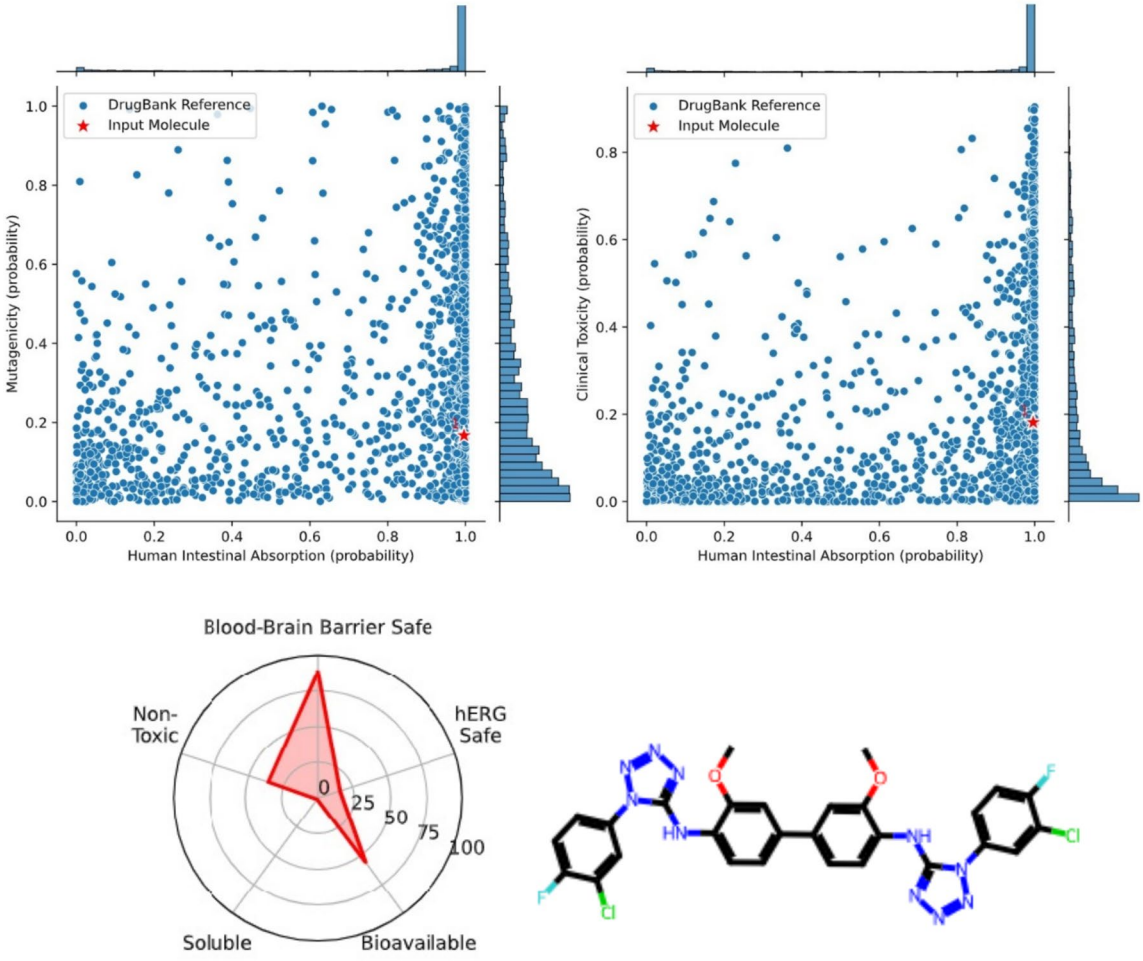

Fig. 4. Example prediction of mutagenicity and clinical toxicity for derivative **1** using ADMET-AI platform.

Carcinogenicity prediction scores were highly satisfactory, with most derivatives exceeding the 90th percentile. Regarding mutagenicity and clinical toxicity, the evaluated compounds fell within the range of the majority of model-included drugs. The lowest acute toxicity predictions were observed for derivatives **2** and **8** (34.97% and 29.66%, respectively). Comparing these results with reference drugs reveals notable trends. The tested compounds ranked approximately two-fold higher than cisplatin but slightly lower than doxorubicin in percentile scores. Their mutagenicity scores were lower than those of both reference drugs, while carcinogenicity

predictions closely matched cisplatin but differed from doxorubicin. Acute toxicity scores were closer to those of cisplatin, and none of the derivatives reached the doxorubicin level. Overall, the results were consistent across the studied group, indicating a favorable toxicity profile.

The second evaluation utilized the ProTox 3.0 model[44] for comparison. As expected, different predictive models yield varying results; however, such analyses are valuable for identifying consistent trends or significant discrepancies. Overall, toxicity endpoint values remained consistent across the ten studied derivatives. Notably, immunotoxicity predictions differed from other endpoints, and no clear linear trend was observed. Compounds **4**, **5**, and **8** exhibited the highest immunotoxicity scores, yet the entire group demonstrated a low probability of immunotoxicity. Additionally, all derivatives were classified as inactive for cytotoxicity, nutritional toxicity, and most carcinogenicity endpoints. Conversely, the analysis indicated that all compounds, except derivative **10**, were predicted to exhibit mutagenicity. Furthermore, all derivatives were associated with toxic properties related to blood–brain barrier (BBB) permeability, ecotoxicity, and clinical toxicity.

The spider web visualization (see Supplementary Fig. S1 online) indicates that compound **1** does not surpass the average results of the reference active molecules included in this prediction model. No definitive conclusion can be drawn when comparing the studied group to both reference drugs (see Supplementary Table S1 online). Doxorubicin exhibited activity for immunotoxicity, mutagenicity, cytotoxicity, and clinical toxicity, whereas cisplatin showed the opposite profile. Most studied derivatives were inactive for immunotoxicity and cytotoxicity, while doxorubicin remained active. Regarding blood–brain barrier (BBB) permeability and ecotoxicity, only cisplatin was inactive. Nutritional toxicity results were consistent, as all tested derivatives, including the reference drugs, were classified as inactive.

Both predictive models provided positive results for toxicity parameters. In both evaluations, reference drugs were included. However, in silico predictions should be validated through in vitro evaluation.

Lactate Dehydrogenase Assay—cell damage assessment

Lactate dehydrogenase assay (LDH) as a cell death marker was evaluated for synthesized tetrazoles representatives. The compounds were tested at 25, 50, and 100 μM concentrations. As shown in Fig. 5, the LDH test highlighted lower toxicity of the new derivatives against HaCaT cells compared to cancer cell lines.

The LDH release from normal keratinocytes ranged from 28.5% (compound **10**) to 33.4% (compound **7**) at a dose of 100 μM. At lower doses of 50 μM and 25 μM, LDH release ranged from 12.6% (compound **10**) to 26.3% (compound 4) and from 5.8% (compound **7**) to 15.5% (compound **4**), respectively. Overall, the results align with MTT assay findings, showing approximately two-fold higher toxicity in cancer cell lines at 100 μM and 50 μM. However, this trend was not observed at the lowest dose. Interestingly, a similar "two-fold" effect was noted in the A549 (human lung adenocarcinoma) cell line, despite none of the compounds achieving a selectivity index (SI) of 1.5 in the MTT test. The strongest cytotoxic effect was observed in SW620 (colorectal cancer) and HTB-140 (human melanoma) cell lines, reaching 68.9% LDH release with compound **7** at 100 μM. Other derivatives also exhibited high LDH release levels (≥ 55%, 100 μM), including all tested compounds for HTB-140, compounds **3**, **4**, **5**, and **8** for A549, compound **4** for HeLa, and all tested derivatives for SW620 except compound **3**. At the lowest dose (25 μM), the "two-fold" potency trend was maintained for HTB-140 and SW620 cell lines when compounds **5**, **7**, **8**, and **10** were applied.

Overall, these findings are promising and warrant further investigation. Selected derivatives have been advanced for additional testing.

Apoptotic activity

To explain the basic mechanism of cell death induction, the effect of derivatives **3**, **4**, **5**, **7**, **8**, and **10** on early and late apoptosis using Annexin V FITC/7-AAD flow cytometry analysis was investigated. As shown (Figs. 6, 7a–e),

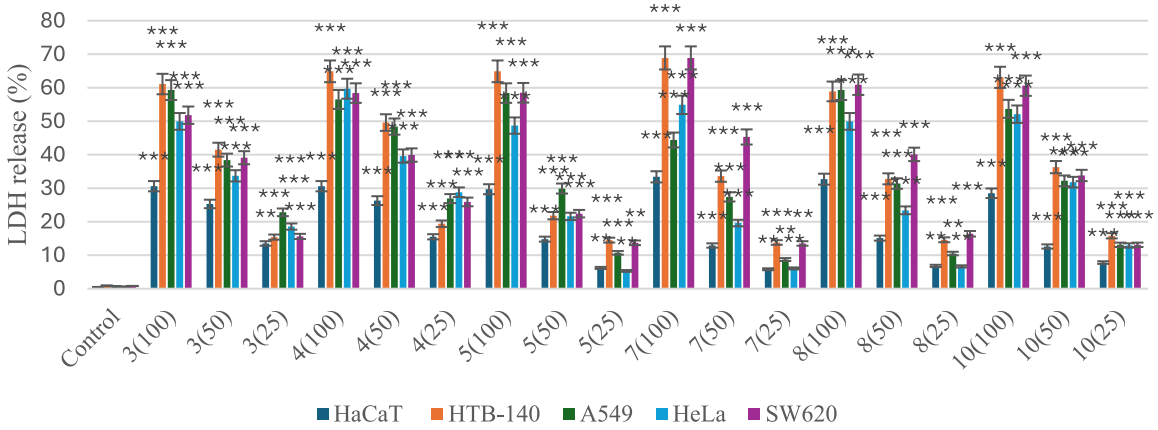

Fig. 5. LDH release as a marker of cell death in the HaCaT, HTB-140, A549, HeLa, SW620 cells, treated for 72 h with different concentrations of derivatives **3**, **4**, **5**, **7**, **8**, and **10** (100 μM, 50 μM, and 25 μM). Data are expressed as the mean ± SD from three independent experiments, performed in triplicate. ***$p \leq 0.001$, **$p \leq 0.01$, compared to the control.

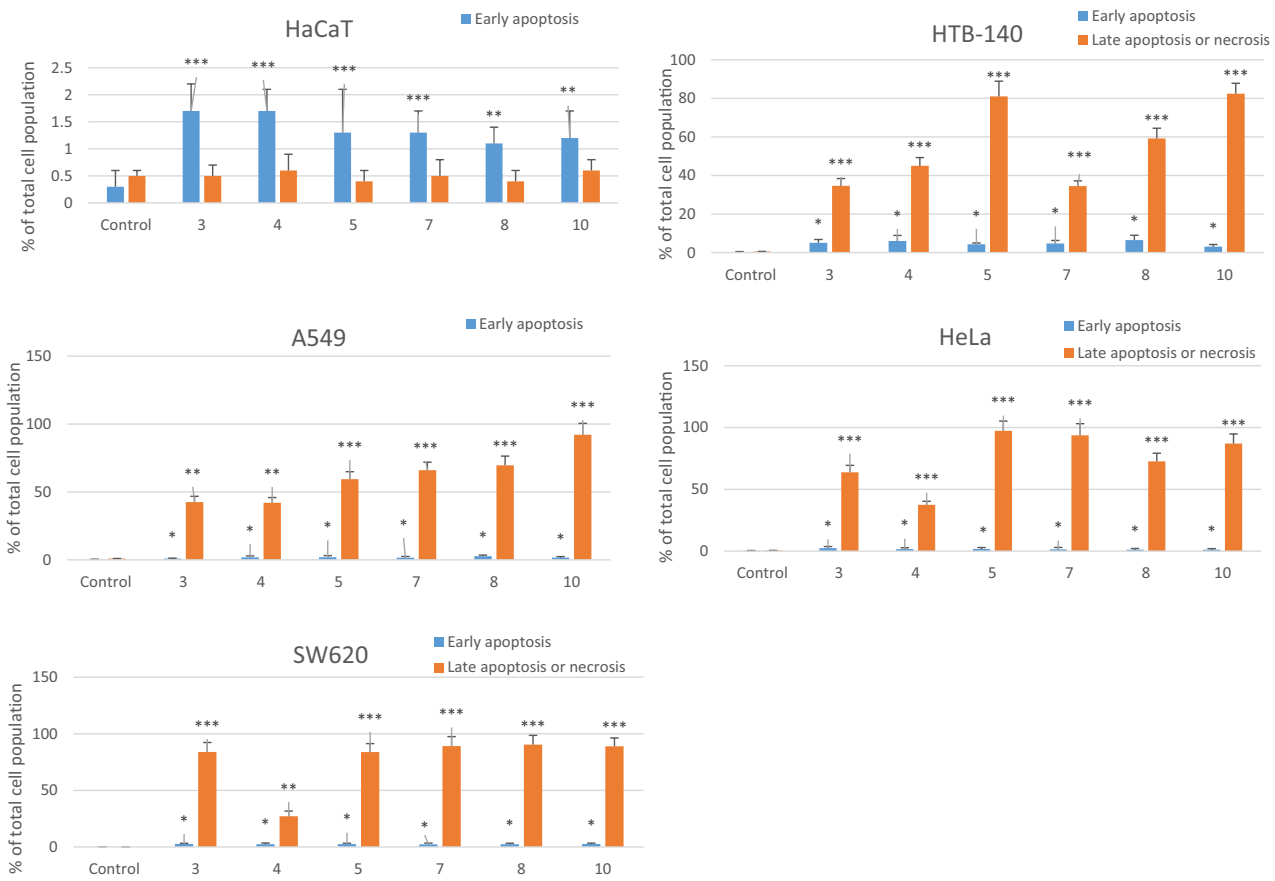

Fig. 6. The effect of compounds **3**, **4**, **5**, **7**, **8**, and **10** on early and late apoptosis or necrosis in HaCaT, HTB-140, A549, HeLa, and SW620 cells as detected by flow cytometry. Data are expressed as % of cells at an early stage of apoptosis and as % of cells at late stage apoptosis or necrotic cells. Data are expressed as means ± SD. ***$p \leq 0.001$, **$p \leq 0.01$, *$p \leq 0.05$ as compared to control.

the studied derivatives applied in their IC_{50} concentrations induced significantly late apoptosis or necrosis in cancerous cells compared to controls.

Selected derivatives induced early apoptosis in HaCaT cells compared to the control; however, the percentage remained low, reaching only 1.7% for compounds **3** and **4** (control: 0.3%). No late apoptosis or necrosis was observed in normal human keratinocytes. In cancer cell lines, early apoptosis was generally weak. The highest early apoptosis rate (6.5%, control: 0.3%) was observed for derivative **8** in HTB-140 cells. Overall, this weak early apoptotic effect was consistent across all derivatives and cancer cell lines.

Late apoptosis and necrosis induction showed notable trends. All tested derivatives exhibited a pro-apoptotic effect in cancer cell lines, though compounds **3** and **4** (bearing 3-fluorophenyl and 3-chlorophenyl substituents) were less active than others. For example, in HeLa cells, compound **4** induced late apoptosis/necrosis in 37.5% of the population ($IC_{50} = 24.4 \pm 6.5$ µM). Other compounds significantly increased late apoptosis in cancer cells. In A549 cells, compound **10** (3-(trifluoromethyl)phenyl substituent) exhibited the highest late-apoptotic activity, reaching 92.1% ($IC_{50} = 33.6 \pm 7.3$ µM). Derivatives **5**, **7**, and **8** induced late apoptosis at approximately 60%. Similarly, compound **10** showed high activity in HTB-140 cells (82.4%, $IC_{50} = 27.9 \pm 2.6$ µM), followed by compound **5** (2-phenylethyl moiety) at 81%. In HeLa cells, all tested compounds except **4** demonstrated late-apoptotic activity above 60%, ranging from 63.8% to 97.3%. Similarly, in SW620 cells, all derivatives except **4** exhibited strong late apoptosis induction, with values ranging from 83.8 to 90.4%. These findings indicate that, despite variations in substituents, the tested group (excluding compound **4**) demonstrated consistently high late-apoptotic activity.

The obtained results align with IC_{50} values determined for each cell line using the MTT assay.

Molecular docking

Among the key pathways involved in the regulation of apoptosis, notable groups of proteins include the Bcl-2 protein family, the JAK/STAT3 pathway, and the PI3K/AKT/mTOR signaling pathway. In this study, we conducted an in silico screening targeting three proteins from the Bcl-2 family, focusing on those with available crystallographic structures co-crystallized with their inhibitors. Specifically, we examined the following proteins in the complex with naturally bound, co-crystallized molecules (native ligands): Apoptosis Regulator Bcl-2 (**4lvt,**

a) HaCaT (from left side: control, **3**, **4**, **5**, **7**, **8**, **10** respectively).

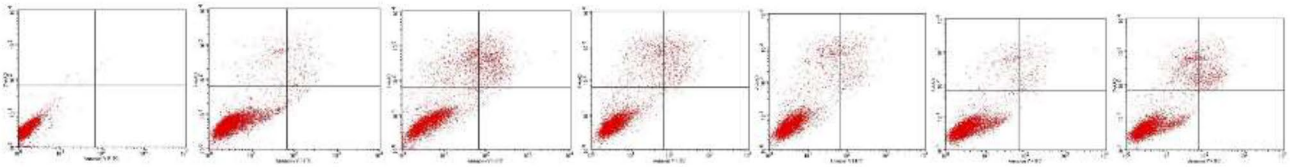

b) HTB-140 (from left side: control, **3**, **4**, **5**, **7**, **8**, **10** respectively).

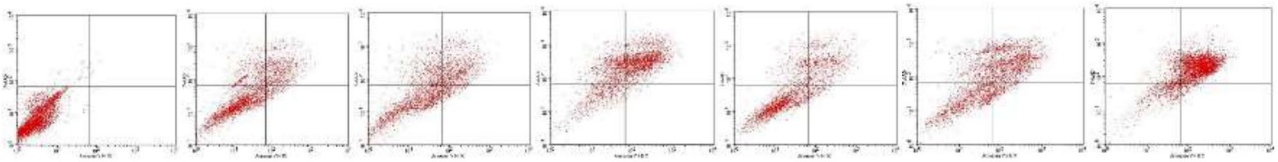

c) A549 (from left side: control, **3**, **4**, **5**, **7**, **8**, **10** respectively).

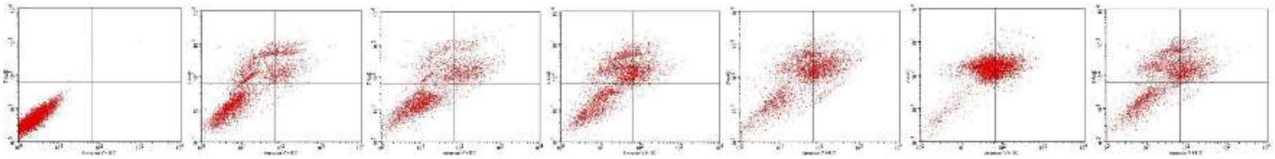

d) HeLa (from left side: control, **3**, **4**, **5**, **7**, **8**, **10** respectively).

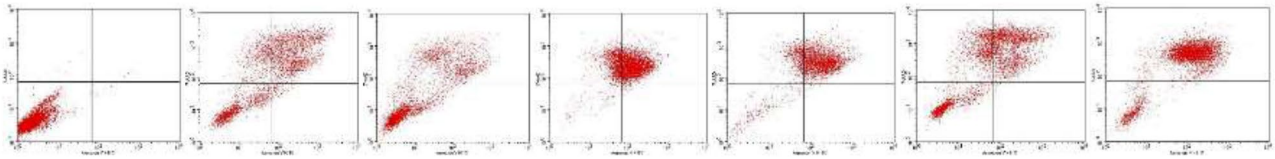

e) SW620 (from left side: control, **3**, **4**, **5**, 7, **8**, **10** respectively).

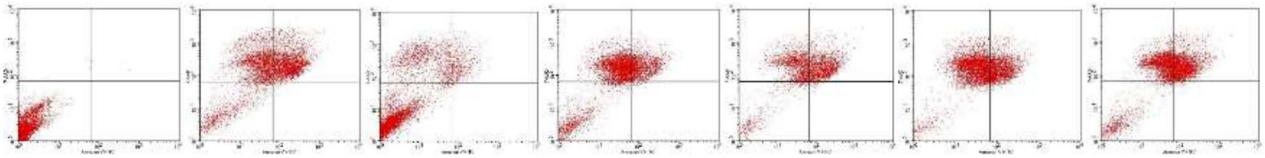

Fig. 7. (**a**–**e**) Diagrams of FITC-Annexin V/7-AAD flow cytometry for HaCaT, HBT-140, A549, HeLa, and SW620 cells. Cells were incubated for 72 h with compounds **3**, **4**, **5**, **7**, **8**, and **10** used in their IC_{50} concentrations. Then cells were harvested, stained with Annexin V-FITC and 7-AAD, and analyzed using flow cytometry. The lower right quadrant represents early apoptotic cells (Annexin V-FITC positive and 7-AAD negative staining). The upper right and upper left quadrants contain late-stage apoptotic cells or necrotic cells (Annexin V-FITC positive and 7-AAD positive and Annexin V-FITC negative and 7-AAD positive staining, respectively).

6o0p, 6o0o), Bcl-2-Like Protein 1 (**1ysg, 2yxj**), and Induced Myeloid Leukemia Cell Differentiation Protein Mcl-1 (**8av9, 6uab, 6fs0**). The crystallographic data and associated inhibitors for these targets are presented in the supplement (see Supplementary Table S2 online), with information sourced from the Protein Data Bank and DrugBank.

The results of the docking study allowed us to assess the interactions between the selected proteins and their inhibitors, shedding light on their binding mechanisms and providing insights into potential therapeutic targets. The study was conducted for ten investigated molecules, and all results are presented in Table 3. It presents the binding affinity results for the top ten docked poses of each ligand within the active site of the respective protein, along with a comparison to the co-crystallized reference molecule. The mean binding score represents the average binding affinity across the ten docked poses, while the standard deviation (std) reflects the variability in the binding affinity values. These results highlight the overall strength and stability of the ligand–protein interactions, as well as the variability among different poses. The more consistent the binding affinity, the stronger and more stable the interaction between the ligand and protein, which can provide insights into the most favorable interactions for potential therapeutic targets.

The native ligands for the analyzed proteins exhibited scoring values ranging from − 16.40 kcal/mol (6FS0, Induced Myeloid Leukemia Cell Differentiation Protein Mcl-1) to − 6.79 kcal/mol (1YSG, Bcl-2-like protein 1),

	Crystal PDB ID							
	4LVT	6O0P	6O0O	1YSG	2YXJ	8AV9	6UAB	6FS0
	Predicted binding score [kcal/mol] (↓)							
Native molecule	− 10.15	**− 10.87**	− 8.85	− 6.79	− 9.79	**− 16.30**	− 5.00	**− 16.40**
	10 poses predicted binding score (mean|std) [kcal/mol]							
1	− 9.27|0.31	− 9.45|0.37	− 8.56|0.35	− 8.16|0.35	− 9.75|0.26	− 9.21|0.45	**− 7.56|0.31**	**− 9.26|0.33**
2	− 9.39|0.41	− 9.33|0.35	− 7.83|0.19	− 7.42|0.40	− 9.44|0.40	− 7.77|0.40	− 7.32|0.29	− 8.23|0.19
3	− 9.35|0.38	− 9.02|0.26	− 8.15|0.27	− 7.46|0.40	− 9.46|0.35	− 9.27|0.28	− 7.31|0.27	− 8.92|0.37
4	− 8.78|0.27	− 8.84|0.30	− 7.93|0.17	− 7.48|0.38	− 9.52|0.26	− 8.67|0.45	− 7.48|0.27	− 8.76|0.21
5	**− 10.29|0.23**	− 10.27|0.53	− 8.81|0.25	**− 9.19|0.65**	**− 10.44|0.25**	− 9.26|0.11	− 6.60|0.21	− 7.93|0.33
6	− 8.87|0.24	**− 10.28|0.27**	− 8.18|0.26	− 7.63|0.25	− 9.97|0.16	− 9.16|0.20	− 7.2|0.26	− 8.84|0.13
7	− 9.29|0.19	− 8.61|0.14	− 8.20|0.26	− 7.14|0.16	− 9.61|0.32	− 8.33|0.27	− 7.27|0.36	− 8.22|0.29
8	− 8.94|0.38	− 8.64|0.44	− 7.60|0.24	− 7.28|0.18	− 8.96|0.38	− 7.63|0.36	− 7.13|0.15	− 8.12|0.28
9	− 9.37|0.24	− 9.11|0.45	− 8.04|0.15	− 7.74|0.39	− 9.76|0.17	− 8.15|0.35	− 7.33|0.37	− 8.62|0.35
10	− 8.49|0.16	− 8.91|0.11	− 7.84|0.21	− 7.31|0.36	− 9.17|0.32	− 7.99|0.14	− 7.55|0.22	− 8.62|0.15

Table 3. Comparison of average AutoDock SMINA results for native and studied molecules. Significant values are in bold.

reflecting strong binding interactions. The lowest values (− 16.40 and − 16.30 kcal/mol) were observed for the 6FS0 and 8AV9 structures, suggesting particularly high specificity and binding stability in these systems.

The tested compounds demonstrated diverse scoring values, many of which were close to the native results. For protein 4LVT (Apoptosis Regulator Bcl-2), the best binding was predicted in derivative **5** (− 10.29 kcal/mol), a value similar to the native ligand (− 10.15 kcal/mol). Comparable results were observed for 6O0P, where **5** achieved a score of − 10.27 kcal/mol compared to − 10.87 kcal/mol for the native ligand.

For protein 6FS0 (Induced Myeloid Leukemia Cell Differentiation Protein Mcl-1), the best scores of the tested ligands (− 9.26 kcal/mol for **1**) were significantly weaker than those of the native ligand (− 16.40 kcal/mol), suggesting a lack of complete replication of key interactions in the binding site. Similarly, for 8AV9, the difference between the native ligand and the best pose was approximately 7 kcal/mol. The only potential confusion in this case may arise from the comparison with the 6UAB complex, where the native ligand performs worse. However, when compared with the other results for Mcl-1, the outcomes are not conclusive. Additionally, given the significant size difference between the native ligand and the studied molecules, the scoring function result may also be biased against Adamantane (see Fig. 8c).

Particular attention was given to the Bcl-2 protein, as its interaction with various inhibitors is critical for understanding its role in apoptosis regulation. A comparison of the docking results for the studied compounds with the native ligands (referent structures) revealed both similarities and differences.

In all three Bcl-2 protein crystals, potential tested inhibitors exhibited docking poses with strong binding scores comparable to those of the native ligands. For example, molecule **5** for each Bcl-2 crystal demonstrated promising binding scores, closely mirroring the native molecule's score. This suggests that these compounds may have similar binding mechanisms to the native ligands, effectively occupying the same binding sites in the Bcl-2 protein.

Despite the similarities in binding scores for some conformations, several other poses displayed weaker results. For example, molecule **10** poses in the Bcl-2 pocket showed significantly weaker binding, with scores ranging from − 8.49 to − 7.84 kcal/mol, suggesting these compounds may not interact as stably with the Bcl-2 protein. These differences could reflect variations in the orientation or conformation of the ligands within the binding site, influencing their stability and potential efficacy as inhibitors.

The tested compounds showed promising results for apoptosis regulator Bcl-2, where the best scoring values were close to those of the native ligands (see Fig. 8a,b). The results for induced myeloid leukemia cell differentiation protein Mcl-1 indicate a limited ability of the tested compounds to replicate native interactions, which may stem from the absence of specific interactions or structural mismatches.

The molecular docking studies were conducted to further explore the potential cytotoxic mechanisms of the studied compounds. The promising results from the apoptosis assay, which indicated a significant number of cells in the late apoptosis stage, were correlated with molecular docking predictions and compared to known Bcl-2 inhibitors (native ligands). The studied compounds demonstrated the ability to form stable complexes with the molecular target, providing a possible explanation for their cytotoxic activity. Furthermore, the complementary in vitro and in silico findings suggest that the future design and synthesis of novel tetrazole derivatives as Bcl-2 inhibitors hold great potential for developing highly cytotoxic agents.

Interleukin-6 Assay

Interleukin-6 (IL-6) is a cytokine that activates inflammatory and autoimmune responses in various diseases, such as pancreatic, prostate, and colon cancers. Elevated levels of IL-6 are observed in advanced and metastatic cancers, where it plays a role in tumor development and progression. All investigated human cell lines were treated with IC_{50} doses of the most potent derivatives **3**, **4**, **5**, **7**, **8**, and **10** (see Fig. 9).

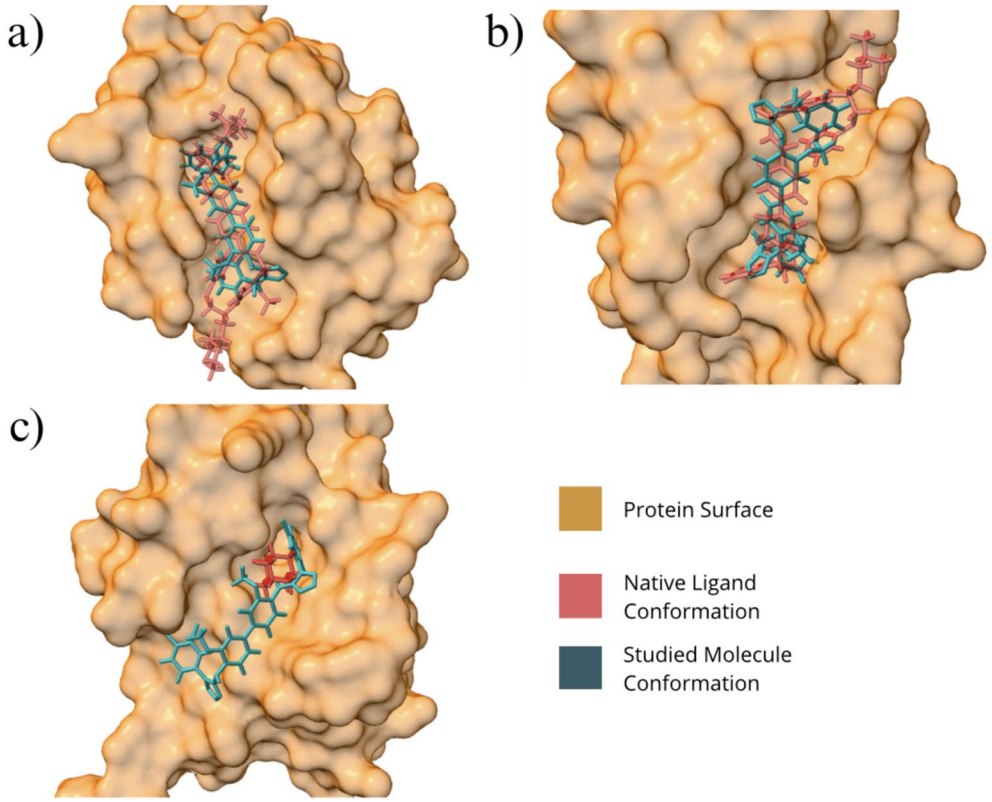

Fig. 8.. 3D visualization of the conformation of the best-docked ligand in the binding pocket compared to the native ligand for (**a**) Apoptosis Regulator Bcl-2|PDB ID: 4LVT|Molecule: **5**, (**b**) Bcl-2 like protein 1|PDB ID: 2YXJ|Molecule: **5**, (**c**) Induced myeloid leukemia cell differentiation protein Mcl-1|PDB ID: 6UAB|Molecule: **1**.

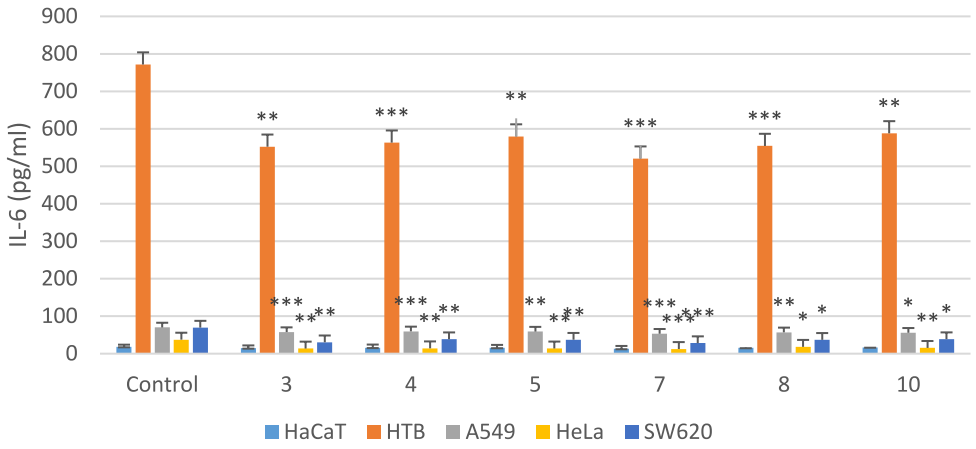

Fig. 9. Effects of tetrazole derivatives on IL-6 levels measured by ELISA test. Data are expressed as the mean ± SD from three independent experiments performed in triplicate. ***$p \leq 0.001$, **$p \leq 0.01$, *$p \leq 0.05$ as compared to control.

Derivative **7** exhibited the most significant effect on HTB-140 cells, reducing interleukin-6 (IL-6) release by over 30% compared to the control. Other compounds demonstrated similar activity levels. In SW620 cells, compound **7** showed the strongest effect among the tested derivatives, reducing IL-6 secretion by 28%. In HeLa cells, all derivatives inhibited IL-6 release by an average of 30%.

In summary, all selected derivatives significantly reduced IL-6 levels in HTB-140, SW620, and HeLa cancer cells. In contrast, no sensitivity was observed in HaCaT and A549 cell lines.

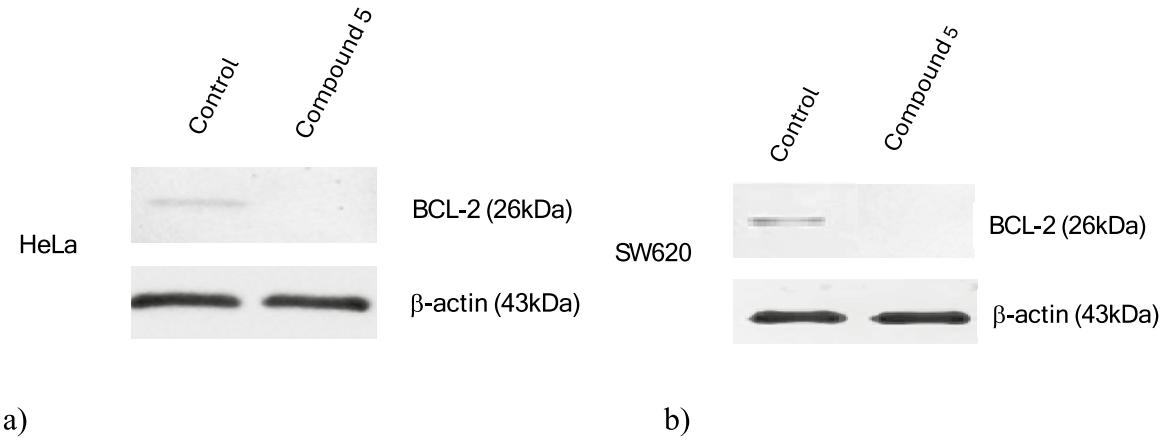

Fig. 10. Effect of compound **5** on Bcl-2 protein expression measured using (**a**) HeLa cervical cancer cell line, (**b**) SW620 colorectal cancer cell line.

Western blot analysis

B-cell lymphoma 2 (Bcl-2) is a key anti-apoptotic protein that resides on mitochondrial membranes. It prevents cells from undergoing programmed cell death, acting as a cellular "guardian" that protects the mitochondria by sequestering death-inducing factors. It ensures cell survival under stress.

We have performed western blot analysis using molecule **5** (for each Bcl-2 crystal demonstrated promising binding scores in the molecular docking experiment) and two cancer cell lines based on the apoptotic studies results. When HeLa (cervical cancer) and SW620 (colorectal cancer) cells were treated with compound **5**, western blot analysis revealed a dramatic loss of Bcl-2 protein expression in these cells (see Fig. 10).

This downregulation (or absence) of Bcl-2 upon compound **5** exposure is a striking result, given this protein's role as a protector against apoptosis. This result suggests that compound **5** effectively knocks out the cells' Bcl-2-mediated survival mechanism, leaving the cells with significantly reduced anti-apoptotic defenses. In practical terms, the treated cancer cells no longer produce (or maintain) Bcl-2 protein at normal levels, which implies they have become much more prone to apoptosis. For additional information, full-length images, and technical procedures from the analysis, please see Supplementary Figs. S12–S16, Tables S3–10, online, and Sect. 3.7.

Discussion

Several derivatives demonstrated selective cytotoxicity against cancer cells, with selectivity indexes (SI) exceeding 1.5 for HTB-140, HeLa, and SW620 cell lines. Compound **7** (benzyl-substituted) exhibited the strongest activity, significantly inducing late apoptosis and necrosis in HeLa cells. Compound **10** (trifluoromethyl-substituted) displayed the highest late-apoptotic activity in A549 cells. In silico toxicity predictions correlated with in vitro findings, indicating acceptable toxicity profiles compared to the reference drugs cisplatin and doxorubicin.

Tested compounds, particularly compound **5**, showed promising activity as Bcl-2 protein inhibitor, exhibiting binding affinities comparable to those of native ligands. Across all three Bcl-2 protein crystals, the potential inhibitors demonstrated docking poses with strong binding scores. For example, molecule **5** consistently displayed binding scores closely matching those of the native ligand. The western blot result suggests that compound **5** effectively knocks out the cells' Bcl-2-mediated survival mechanism, leaving the cells with significantly reduced anti-apoptotic defenses. Furthermore, the derivatives effectively reduced IL-6 levels in selected cancer cell lines, with compound **7** showing the highest inhibitory effect.

The synthesized tetrazole derivatives exhibit promising anticancer potential, demonstrating favorable selectivity and apoptotic activity. These findings underscore the potential of utilizing hazardous substrates to develop novel anticancer agents in alignment with green chemistry principles. The results suggest that substituted tetrazole derivatives could serve as promising Bcl-2 protein inhibitors capable of regulating apoptosis in melanoma, cervical, and colorectal cancer cells. Further studies are warranted to optimize lead compounds and evaluate their therapeutic efficacy in vivo.

Materials and methods

Chemistry

Triethylamine (503 µl, 3.75 mmol, 1–3 drops) was added to a suspension of a corresponding thiourea substrate (1.25 mmol), sodium azide (244 mg, 3.75 mmol), and mercuric chloride (373 mg, 1.38 mmol) in 20 mL of dry DMF. The resulting suspension was stirred for 6 h at room temperature or until TLC indicated complete consumption of the starting material. The suspension was filtered through a pad of celite, and washed with CH_2Cl_2. The filtrate was diluted with water, and extracted with 3×15 mL of CH_2Cl_2. The combined organic fractions were dried over $MgSO_4$, filtered, and concentrated under reduced pressure. The resulting residue was purified by silica gel chromatography using CH_2Cl_2/MeOH (0.9:0.1) as eluent.

1-(3-chloro-4-fluorophenyl)-N-[4-[4-[[1-(3-chloro-4-fluorophenyl)tetrazol-5-yl]amino]-3-methoxyphenyl]-2-methoxyphenyl]tetrazol-5-amine (1)
Yield 68%. White solid. Mp 152–154 °C. ^{1}H NMR (500 MHz, DMSO-d_6) δ: 9.48 (s, 2H, NH), 7.98 (dd, J = 2.5 Hz, 6.5 Hz, 2H), 7.74 (d, J = 8.0 Hz, 2H), 7.69–7.66 (m, 4H), 7.63 (dd, J = 2.0 Hz, 8.0 Hz, 2H), 7.41 (t, J = 9.0 Hz, 2H), 3.95 (s, 6H, 2xOCH$_3$). ^{13}C NMR (125 MHz, DMSO-d_6) δ: 154.9, 152.7, 152.5 (d, $^{1}J_{C\text{-}F}$ = 240.0 Hz), 143.4, 137.0 (d, $^{3}J_{C\text{-}F}$ = 2.5 Hz), 129.5, 120.7, 119.8, 119.3, 119.3 (d, $^{2}J_{C\text{-}F}$ = 17.5 Hz), 118.3 (d, $^{3}J_{C\text{-}F}$ = 7.5 Hz), 117.1 (d, $^{2}J_{C\text{-}F}$ = 22.5 Hz), 111.9, 56.4. HRMS (ESI) m/z 637.11886 calc. for $C_{28}H_{20}Cl_2F_2N_{10}O_2$ [M + H] + ; found 637.11890.

1-(3-bromophenyl)-N-[4-[4-[[1-(3-bromophenyl)tetrazol-5-yl]amino]-3-methoxyphenyl]-2-methoxyphenyl] tetrazol-5-amine (2)
Yield 87%.White solid. Mp 148–149 °C. ^{1}H NMR (500 MHz, DMSO-d_6) δ: 9.41 (s, 2H, NH), 8.00 (t, J = 2.0 Hz, 2H), 7.71–7.70 (m, 2H), 7.64 (d, J = 8.0 Hz, 2H), 7.59 (t, J = 8.0 Hz, 2H), 7.55 (d, J = 2.0 Hz, 2H), 7.49 (dd, J = 1.5 Hz, 8.0 Hz, 2H), 7.20–7.18 (m, 2H), 3.91 (s, 6H, 2xOCH$_3$). ^{13}C NMR (125 MHz, DMSO-d_6) δ: 154.8, 152.6, 144.2, 141.4, 135.1, 130.8, 129.2, 128.4, 124.4, 122.1, 120.9, 119.5, 111.1, 56.3. HRMS (ESI) m/z 689.03667 calc. for $C_{28}H_{22}Br_2N_{10}O_2$ [M + H] + ; found 689.03706.

1-(3-fluorophenyl)-N-[4-[4-[[1-(3-fluorophenyl)tetrazol-5-yl]amino]-3-methoxyphenyl]-2-methoxyphenyl] tetrazol-5-amine (3)
Yield 72%.White solid. Mp 153–156 °C. ^{1}H NMR (500 MHz, DMSO-d_6) δ: 9.51 (s, 2H, NH), 7.74 (d, J = 8.5 Hz, 2H), 7.68–7.62 (m, 6H), 7.53–7.51 (m, 2H), 7.39–7.35 (m, 2H), 6.86–6.82 (m, 2H), 3.95 (s, 6H, 2xOCH$_3$). ^{13}C NMR (125 MHz, DMSO-d_6) δ: 163.4, 161.5, 153.8 (d, $^{1}J_{C\text{-}F}$ = 282.5 Hz), 143.4, 141.6 (d, $^{3}J_{C\text{-}F}$ = 11.3 Hz), 130.5 (d, $^{3}J_{C\text{-}F}$ = 10.0 Hz), 129.5, 120.8, 119.8, 113.8 (d, $^{4}J_{C\text{-}F}$ = 2.5 Hz), 111.9, 108.4 (d, $^{2}J_{C\text{-}F}$ = 21.3 Hz), 104.8 (d, $^{2}J_{C\text{-}F}$ = 27.5 Hz), 56.4. HRMS (ESI) m/z 569.19680 calc. for $C_{28}H_{22}F_2N_{10}O_2$ [M + H] + ; found 569.19721.

1-(3-chlorophenyl)-N-[4-[4-[[1-(3-chlorophenyl)tetrazol-5-yl]amino]-3-methoxyphenyl]-2-methoxyphenyl] tetrazol-5-amine (4)
Yield 81%.White solid. Mp 151–152 °C. ^{1}H NMR (500 MHz, DMSO-d_6) δ: 9.41 (s, 2H, NH), 7.93 (t, J = 2.0 Hz, 2H), 7.80–7.70 (m, 2H), 7.72–7.71 (m, 2H), 7.63 (d, J = 8.0 Hz, 2H), 7.44 (dd, J = 2.0 Hz, 8.5 Hz, 2H), 7.38 (d, J = 2.0 Hz, 2H), 7.30 (t, J = 8.0 Hz, 2H), 3.92 (s, 6H, 2xOCH$_3$). ^{13}C NMR (125 MHz, DMSO-d_6) δ: 154.8, 152.5, 144.2, 141.4, 134.7, 131.7, 128.4, 127.3, 123.7, 121.7, 120.2, 119.1, 110.2, 56.3. HRMS (ESI) m/z 601.13770 calc. for $C_{28}H_{22}Cl_2N_{10}O_2$ [M + H] + ; found 601.13771.

N-[2-methoxy-4-[3-methoxy-4-[[1-(2-phenylethyl)tetrazol-5-yl]amino]phenyl]phenyl]-1-(2-phenylethyl)tetrazol-5-amine (5)
Yield 79%.White solid. Mp 167–169 °C. ^{1}H NMR (500 MHz, DMSO-d_6) δ: 7.56–7.53 (m, 5H), 7.32–7.29 (m, 4H), 7.23–7.21 (m, 5H), 6.86 (t, J = 5.5 Hz, 2H), 3.90 (s, 6H, 2xOCH$_3$), 3.51–3.47 (m, 4H, 2xCH$_2$), 2.88 (t, J = 7.5 Hz, 4H, 2xCH$_2$). ^{13}C NMR (125 MHz, DMSO-d_6) δ: 155.7, 154.6, 142.9, 139.3, 129.1, 128.7, 128.3, 126.1, 121.1, 119.6, 111.6, 56.2, 44.9, 34.8. HRMS (ESI) m/z 589.27825 calc. for $C_{32}H_{32}N_{10}O_2$ [M + H] + ; found 589.27830.

N-[2-methoxy-4-[3-methoxy-4-[[1-(1-phenylethyl)tetrazol-5-yl]amino]phenyl]phenyl]-1-(1-phenylethyl)tetrazol-5-amine (6)
Yield 61%.White solid. Mp 164–166 °C. ^{1}H NMR (500 MHz, DMSO-d_6) δ: 7.61–7.54 (m, 5H), 7.41–7.39 (m, 4H), 7.35–7.32 (m, 5H), 7.25–7.21 (m, 2H), 4.96–4.90 (m, 2H, 2xCH), 3.95 (s, 6H, 2xOCH$_3$), 1.47 (d, J = 7.0 Hz, 6H, 2xCH$_3$). ^{13}C NMR (125 MHz, DMSO-d_6) δ: 155.2, 154.7, 144.7, 143.0, 129.1, 128.2, 126.7, 126.0, 121.2, 119.5, 111.7, 56.1, 53.3, 22.9. HRMS (ESI) m/z 589.27825 calc. for $C_{32}H_{32}N_{10}O_2$ [M + H] + ; found 589.27843.

1-Benzyl-N-[4-[4-[(1-benzyltetrazol-5-yl)amino]-3-methoxyphenyl]-2-methoxyphenyl]tetrazol-5-amine (7)
Yield 90%.White solid. Mp 148–150 °C. ^{1}H NMR (500 MHz, DMSO-d_6) δ: 759–7.53 (m, 5H), 7.41 (t, J = 6.0 Hz, 2H), (7.35–7.33 (m, 7H), 7.26–7.23 (m, 2H), 4.48 (d, J = 6.0 Hz, 4H, 2xCH$_2$), 3.93 (s, 6H, 2xOCH$_3$). ^{13}C NMR (125 MHz, DMSO-d_6) δ: 155.9, 154.6, 143.0, 139.3, 129.1, 128.2, 127.1, 126.9, 121.1, 119.6, 111.7, 56.2, 46.6. HRMS (ESI) m/z 561.24695 calc. for $C_{30}H_{28}N_{10}O_2$ [M + H] + ; found 561.24699.

1-(4-Iodophenyl)-N-[4-[4-[[1-(4-iodophenyl)tetrazol-5-yl]amino]-3-methoxyphenyl]-2-methoxyphenyl]tetrazol-5-amine (8)
Yield 81%.White solid. Mp 144–146 °C. ^{1}H NMR (500 MHz, DMSO-d_6) δ: 9.59 (s, 2H, NH), 7.67 (d, J = 1.5 Hz, 2H), 7.64 -7.61 (m, 6H), 7.58–7.54 (m, 6H), 3.93 (s, 6H, 2xOCH$_3$). ^{13}C NMR (125 MHz, DMSO-d_6) δ: 154.9, 153. 0, 143.6, 140.1, 137.5, 129.4, 120.9, 120.6, 119.9, 112.2, 85.2, 56.5. HRMS (ESI) m/z 785.00894 calc. for $C_{28}H_{22}I_2N_{10}O_2$ [M + H] + ; found 785.00919.

1-(3,4-Dichlorophenyl)-N-[4-[4-[[1-(3,4-dichlorophenyl)tetrazol-5-yl]amino]-3-methoxyphenyl]-2-methoxyphenyl]tetrazol-5-amine (9)
Yield 77%.White solid. Mp 139–141 °C. ^{1}H NMR (500 MHz, DMSO-d_6) δ 9.53 (s, 2H, NH), 8.08 (d, J = 2.5 Hz, 2H), 7.92 (d, J = 8.5 Hz, 2H), 7.58 (d, J = 8.5 Hz, 2H), 7.52 (dd, J = 2.5 Hz, 9.0 Hz, 2H), 7.35 (d, J = 2.0 Hz, 2H), 7.29 (dd, J = 2.0 Hz, 8.0 Hz, 2H), 3.94 (s, 6H, 2xOCH$_3$). ^{13}C NMR (125 MHz, DMSO-d_6) δ: 154.9, 152.7, 152.4, 143.5, 140.0, 137.0, 130.1, 126.8, 125.6, 124.3, 123.1, 118.3, 110.0, 55.9. HRMS (ESI) m/z 652.4379 calc. for $C_{28}H_{20}Cl_4N_{10}O_2$ [M + H] + ; found 652.9987.

N-[2-methoxy-4-[3-methoxy-4-[[1-[3-(trifluoromethyl)phenyl]tetrazol-5-yl]amino]phenyl]phenyl]-1-[3-(trifluoromethyl)phenyl]tetrazol-5-amine (10)
Yield 83%. White solid. Mp 162–165 °C. ^{1}H NMR (500 MHz, DMSO-d_6) δ: 9.87 (bs, 2H, NH), 8.14 (s, 2H), 8.00 (d, J = 8.5 Hz, 2H,), 7.70–7.67 (m, 4H), 7.60 (d, J = 8.0 Hz, 2H), 7.55 (t, J = 8.0 Hz, 2H), 7.31 (d, J = 8.0 Hz, 2H), 3.93 (s, 6H, 2xOCH$_3$). ^{13}C NMR (125 MHz, DMSO-d_6) δ: 155.0, 153.0, 143.7, 141.0, 130.2, 129.7 (q, $^{2}J_{C\text{-}F}$ = 31.3 Hz), 129.5, 124.4 (q, $^{1}J_{C\text{-}F}$ = 271.3 Hz), 121.7, 120.8, 119.9, 118.2, 114.2 (q, $^{3}J_{C\text{-}F}$ = 5.0 Hz), 112.2, 56.5. HRMS (ESI) m/z 669.19042 calc. for $C_{30}H_{22}F_6N_{10}O_2$ [M + H] +; found 669.19110.

Apparatus, materials, and analysis
The reagents were supplied from Alfa Aesar (Haverhill, MA, USA) or Sigma Aldrich (Saint Louis, MO, USA). Organic solvents (acetonitrile, DMF, chloroform, and methanol) were supplied from POCh (Polskie Odczynniki Chemiczne, Gliwice, Poland). All chemicals were of analytical grade. Before use, dried DMF and acetonitrile were kept in crown cap bottles over anhydrous phosphorus pentoxide (Carl Roth, Karlsruhe, Germany). The NMR spectra were recorded on a Bruker AVANCE DMX400 (Bruker, Billerica, MA, USA) spectrometer, operating at 300 MHz (^{1}H NMR) and 75 MHz (^{13}C NMR). The chemical shift values are expressed in ppm relative to TMS as an internal standard. A Nexera X3 system coupled with an LCMS-9030 quadrupole time-of-flight mass spectrometer (Shimadzu Corporation, Kyoto, Japan) was used for FIA-MS. The mobile phase was 0.1% formic acid in methanol. The pump was operated at 0.2 mL/min. Samples were dissolved in CH_2Cl_2, sonicated, vortexed, centrifuged at 6000 rpm to obtain clear solution, which was next diluted in mobile phase. The injection volume of the samples was adjusted in the range of 0.1–1 µL for optimal signal intensity. The ESI positive mode was used with an interface voltage of + 4.0 kV. The temperatures of the interface, desolvation line and heat block were set at 300, 250 and 400 °C, respectively. The flow rates of the nebulizer gas and drying gas were set at 1 and 10 L/min, respectively. In the experiment, MS data were acquired in the range of 100–1000 m/z with 250 ms event time.

In silico toxicological properties
This paper examined target compounds using two prediction models for their toxicological and other physicochemical parameters. The ADMET-AI platform and the ProTox 3.0 model were used to compare results.

In silico molecular docking studies
To investigate the interaction between studied molecules with the Bcl-2 protein family, we performed pocket-based molecular docking of 10 studied molecules against 8 different crystal structures of the receptor, each featuring a defined active site and a confirmed inhibitor of the receptor under study (4LVT, 6O0P, 6O0O, 1YSG, 2YXJ, 8AV9, 6UAB, 6FSO)[45–50]. Molecular docking was performed using the classical software AutoDock Smina 1.1.2[51], targeting the native ligand pocket with an additional amount of buffer space measuring 4 Å. Subsequently, the docking scoring function results were compared with the results for native ligands.

Cytotoxic activity

Cell cultures
Cell lines HBT-140 (human melanoma), A549 (human lung adenocarcinoma), HeLa (cervical cancer), and SW620 (colorectal cancer), and the normal cell line HaCaT (immortalized human keratinocytes) were purchased from American Type Culture Collection (Rockville, USA), and cultured in Dulbecco's Modified Eagle's Medium (DMEM) supplemented with 1% antibiotics (penicillin and streptomycin) and 10% heat-inactivated FBS-fetal bovine serum (Gibco Life Technologies, USA) at 37 °C and 5% CO2 atmosphere. Cells were passaged using trypsin–EDTA (Gibco Life Technologies, USA) and cultured in 24-well or 96-well plates (1×10^4 cells per well). Experiments were conducted in DMEM with 2% FBS.

MTT assay—cell viability assessment
The cell viability was assessed by determination of 3-(4,5-dimethylthiazol-2-yl)-2,5-diphenyltetrazolium bromide salt (MTT) conversion by mitochondrial dehydrogenase[52,53]. The cells were incubated for 72 h in 96-well plates with different concentrations of tested compounds and subsequently for another 4 h with 0.5 mg/mL of MTT solution, which was converted in living cells by mitochondrial dehydrogenase into insoluble formazan. The dye was then solubilized in 0.04 M HCl in absolute isopropanol. The absorbance of solubilized formazan was measured spectrophotometrically at 570 nm (using Epoch microplate reader, BioTek Inc., USA) equipped with Gen5 software (BioTech Instruments, Inc., Biokom). Cell viability was presented as a percent of reduced MTT in treated cells versus control cells (incubated in serum-free DMEM without tested compounds). The relative MTT level (%) was calculated as [A]/[B] × 100, where [A] is the absorbance of the test sample and [B] is the absorbance of the control sample containing the untreated cells. A decreased relative MTT level indicates decreased cell viability.

LDH assay

As a marker of cell death, the release of lactate dehydrogenase (LDH) from the cytosol to the culture medium (cellular membrane integrity assessment) was used. The assay was performed after 72 h incubation of cells in 96-well plates with investigated compounds as described before[35,36]. The activity of lactate dehydrogenase (LDH) released from the cytosol of damaged cells to the supernatant was measured according to the protocol of the cytotoxicity detection kit LDH test described by the manufacturer (Roche Diagnostics, Germany). An absorbance was measured at 490 nm using a microplate reader (using Epoch microplate reader, BioTek Inc., USA) equipped with Gen5 software (BioTech Instruments, Inc., Biokom). Compounds-mediated cytotoxicity expressed as the LDH release (%) was determined by the following equation: [(A test sample – A low control)/

(A high control – A low control)] × 100% (A-absorbance); where "low control" were cells in DMEM with 2% FBS without tested compounds and "high control" were cells incubated in DMEM with 2% FBS with 1% Triton X-100 (100% LDH release).

Apoptotic activity

Apoptosis Detection Kit I; BD Biosciences Pharmingen) was used. Cells were preincubated for 72 h with IC_{50} concentrations of tested compounds. The effect of the exposure of HBT-140 (human melanoma), A549 (human lung adenocarcinoma), HeLa (cervical cancer), SW620 (colorectal cancer), and HaCaT (immortalized human keratinocytes) cells to tested compounds was determined by dual staining with Annexin V: FITC and 7-AAD. Annexin V: FITC and 7-AAD were added to the cellular suspension as described in the manufacturer's instructions and a fluorescence sample of 10,000 cells was analyzed by flow cytometry (Becton Dickinson). Cells that were Annexin V: FITC positive and 7-AAD negative were identified as early apoptotic. Cells that were Annexin V: FITC positive and 7-AAD positive were identified as late apoptotic or necrotic.

Interleukin-6 analysis

The Interleukin IL-6 ELISA kit was purchased from Diaclon SAS (Besancon Cedex, France). The HBT-140 (human melanoma), A549 (human lung adenocarcinoma), HeLa (cervical cancer), SW620 (colorectal cancer), and HaCaT (immortalized human keratinocytes) cells were treated with IC_{50} concentration of selected tetrazole derivatives and with IC_{50} cytostatic drugs for 72 h. IL-6 level in cell culture supernatant was measured using enzyme-linked immunosorbent assay following the manufacturer's protocol.

Western blot analysis

After incubation, cells were lysed in ice-cold RIPA buffer containing phosphatase and protease inhibitors (Sigma-Aldrich, Germany), and the resulting lysates were centrifuged at 10,000 RPM for 15 min at 4 °C. Protein concentration was quantified by a standard colorimetric test (BCA Protein Assay Kit), and 15 µL of lysate was resuspended in 5 µL 4 × Laemmli Buffer, centrifuged, vortexed briefly, boiled for 5 min at 95 °C, vortexed and frozen as aliquots at − 70 °C until analysis by 12% SDS-PAGE. Protein in the amount of 40 µg was transferred to nitrocellulose filters and immunoblotted with antibody: BCL-2 (Cell Signaling Technology, MA, USA; 1:1000) and β-actin (1:5000). Peroxidase-conjugated AffiniPure goat anti-rabbit antibody was used as a secondary antibody at a dilution of 1:1000 (Thermo Scientific, USA) Finally, the blots were incubated with chemiluminescent substrate for the detection of HRP (Thermo Scientific, USA) for 5 min. Western blot analyses were quantified using Image Lab 6.1 software after the densitometric scanning of the bands (Bio-Rad, USA). For the raw, not cropped visuals, see Supplementary Fig. S12– S16 online.

Statistical analysis

The results are expressed as the mean ± SD from the indicated number of experiments. Comparisons were made using the Student's t-test. Differences between experimental groups were considered to be statistically significant at $p \leq 005$.

Data availability

Part of the datasets generated and analyzed during the current study are not publicly available due to requests from co-authors (possible patent submission) but are available from the corresponding author on reasonable request.

Received: 21 December 2024; Accepted: 15 May 2025
Published online: 21 May 2025

References

1. Huang, M., Lu, J.-J. & Ding, J. Natural products in cancer therapy: Past, present and future. *Nat. Prod. Bioprospect.* **11**, 5–13 (2021).
2. Sithranga Boopathy, N. & Kathiresan, K. Anticancer drugs from marine flora: An overview. *J. Oncol.* **2010**, 214186 (2010).
3. Ribeiro, F., Costa-Lotufo, L., Loureiro, S. & Pavlaki, M. D. Environmental hazard of anticancer drugs: State of the art and future perspective for marine organisms. *Environ. Toxicol. Chem.* **41**, 1793–1807 (2022).
4. Basak, D., Arrighi, S., Darwiche, Y. & Deb, S. Comparison of anticancer drug toxicities: Paradigm shift in adverse effect profile. *Life (Basel)* **12**, 48 (2021).
5. Anticancer drug | Pharmacology, Mechanisms & Side Effects | Britannica. https://www.britannica.com/science/anticancer-drug.
6. Remesh, A. Toxicities of anticancer drugs and its management. *Int. J. Basic Clin. Pharmacol.* **1**, 2–12 (2012).
7. Liu, L. et al. A new approach to reduce toxicities and to improve bioavailabilities of platinum-containing anti-cancer nanodrugs. *Sci. Rep.* **5**, 10881 (2015).
8. Acheson, D. Carcinogenic properties of orthodianisidine. *Br. Med. J.* **4**, 742–742 (1967).
9. Chung, K.-T., Chen, S.-C. & Claxton, L. D. Review of the Salmonella typhimurium mutagenicity of benzidine, benzidine analogues, and benzidine-based dyes. *Mutat. Res.* **612**, 58–76 (2006).
10. Golka, K., Kopps, S. & Myslak, Z. W. Carcinogenicity of azo colorants: Influence of solubility and bioavailability. *Toxicol. Lett.* **151**, 203–210 (2004).
11. Jasni, M. J. F. et al. Fabrication, characterization and application of laccase-nylon 6,6/Fe3+ composite nanofibrous membrane for 3,3'-dimethoxybenzidine detoxification. *Bioprocess Biosyst. Eng.* **40**, 191–200 (2017).
12. Sun, X. et al. Curcumin reverses benzidine-induced cell proliferation by suppressing ERK1/2 pathway in human bladder cancer T24 cells. *Exp. Toxicol. Pathol.* **68**, 215–222 (2016).
13. Erdoğan, M. et al. Synthesis and characterization of some benzidine-based azomethine derivatives with molecular docking studies and anticancer activities. *Chem. Papers* **77**(11), 6829–6847 (2023).
14. Ibacache, J. A. et al. Synthesis and antiproliferative evaluation of new aminoisoquinolinequinones derived from p-phenylenediamine, benzidine and dapsone. *J. Chem. Pharm. Res.* **9**, 127–134 (2017).

15. Kazmi, M. T., Amir, M., Iqbal, M. A., Rashid, M. & Husain, A. Thiazolobenzamide-naphthalene hybrids as potent anticancer agents compared to doxorubicin: Design, synthesis, SAR, in-silico and toxicity analysis. *Chem. Biodivers.* **21**, e202301662 (2024).
16. Turan-Zitouni, G. et al. Synthesis and evaluation of bis-thiazole derivatives as new anticancer agents. *Eur. J. Med. Chem.* **107**, 288–294 (2016).
17. Kamal, A. et al. Design, synthesis, biological evaluation and QSAR studies of novel bisepipodophyllotoxins as cytotoxic agents. *Bioorg. Med. Chem.* **12**, 4197–4209 (2004).
18. Dakkak, B. E. et al. Unlocking the therapeutic potential of BCL-2 associated protein family: Exploring BCL-2 inhibitors in cancer therapy. *Biomol. Therapeutics* **32**, 267–280 (2024).
19. Pogmore, J. P., Uehling, D. & Andrews, D. W. Pharmacological targeting of executioner proteins: Controlling life and death. *J. Med. Chem.* **64**, 5276–5290 (2021).
20. Um, H.-D. Bcl-2 family proteins as regulators of cancer cell invasion and metastasis: A review focusing on mitochondrial respiration and reactive oxygen species. *Oncotarget* **7**, 5193–5203 (2016).
21. Adams, J. M. & Cory, S. The BCL-2 arbiters of apoptosis and their growing role as cancer targets. *Cell Death Differ* **25**, 27–36 (2018).
22. Trisciuoglio, D. et al. Bcl-2 overexpression in melanoma cells increases tumor progression-associated properties and in vivo tumor growth. *J. Cell. Physiol.* **205**, 414–421 (2005).
23. Choi, J. et al. Bcl-2 promotes invasion and lung metastasis by inducing matrix metalloproteinase-2. *Cancer Res.* **65**, 5554–5560 (2005).
24. Koehler, B. C. et al. Beyond cell death—Antiapoptotic Bcl-2 proteins regulate migration and invasion of colorectal cancer cells in vitro. *PLoS ONE* **8**, e76446 (2013).
25. Ho, J.-N. et al. Bcl-XL and STAT3 mediate malignant actions of gamma-irradiation in lung cancer cells. *Cancer Sci.* **101**, 1417–1423 (2010).
26. Clément, M.-V., Hirpara, J. L. & Pervaiz, S. Decrease in intracellular superoxide sensitizes Bcl-2-overexpressing tumor cells to receptor and drug-induced apoptosis independent of the mitochondria. *Cell Death Differ* **10**, 1273–1285 (2003).
27. Yumol, J., Gabrielli, B., Tayyar, Y., McMillan, N. A. & Idris, A. Smart drug combinations for cervical cancer: Dual targeting of Bcl-2 family of proteins and aurora kinases. *Am. J. Cancer Res.* **10**, 3406–3414 (2020).
28. Hashiguchi, T. et al. Cyclin-dependent kinase-9 Is a therapeutic target in MYC-expressing diffuse large B-cell lymphoma. *Mol. Cancer Ther.* **18**, 1520–1532 (2019).
29. Li, S. et al. Overcoming multi-drug resistance in SCLC: A synergistic approach with venetoclax and hydroxychloroquine targeting the lncRNA LYPLAL1-DT/BCL2/BECN1 pathway. *Mol. Cancer* **23**, 243 (2024).
30. Ebner, J. et al. ABCC1 and glutathione metabolism limit the efficacy of BCL-2 inhibitors in acute myeloid leukemia. *Nat. Commun.* **14**, 5709 (2023).
31. Haston, S. et al. Clearance of senescent macrophages ameliorates tumorigenesis in KRAS-driven lung cancer. *Cancer Cell* **41**, 1242-1260.e6 (2023).
32. Wang, Y. et al. Venetoclax acts as an immunometabolic modulator to potentiate adoptive NK cell immunotherapy against leukemia. *Cell Rep. Med.* **5**, 101580 (2024).
33. He, Y. et al. DT2216-a Bcl-xL-specific degrader is highly active against Bcl-xL-dependent T cell lymphomas. *J. Hematol. Oncol.* **13**, 95 (2020).
34. Kelly, L. M. et al. Targeting a lineage-specific PI3Kγ-Akt signaling module in acute myeloid leukemia using a heterobifunctional degrader molecule. *Nat. Cancer* **5**, 1082–1101 (2024).
35. Szulczyk, D. et al. Synthetic transition from thiourea-based compounds to tetrazole derivatives: Structure and biological evaluation of synthesized new N-(Furan-2-ylmethyl)-1H-tetrazol-5-amine derivatives. *Molecules* **26**, 323 (2021).
36. Szulczyk, D. et al. Cytotoxicity evaluation of Novel bis(2-aminoethyl)amine derivatives. *Molecules* **25**, 2816 (2020).
37. Bielenica, A. et al. Synthesis, cytotoxicity and antimicrobial activity of thiourea derivatives incorporating 3-(trifluoromethyl) phenyl moiety. *Eur. J. Med. Chem.* **101**, 111–125 (2015).
38. Szostek, T. et al. Design and synthesis of menthol and thymol derived ciprofloxacin: influence of structural modifications on the antibacterial activity and anticancer properties. *Int. J. Mol. Sci.* **23**, 6600 (2022).
39. Olejarz, W., Dominiak, A., Żołnierzak, A., Kubiak-Tomaszewska, G. & Lorenc, T. Tumor-derived exosomes in immunosuppression and immunotherapy. *J. Immunol. Res.* **2020**, 6272498 (2020).
40. Madasani, S. et al. Biphenyl backbone-based (Bis)Urea and (Bis)Thiourea derivatives as antimicrobial and antioxidant agents and evaluation of docking studies and ADME properties. *Polycyclic Aromat. Compd.* **3**, 5915–5939 (2022).
41. Strzyga-Łach, P. et al. Proapoptotic effects of halogenated bis-phenylthiourea derivatives in cancer cells. *Arch. Pharm. (Weinheim).* **356**, e2300105 (2023).
42. Sylvester, P. W. Optimization of the tetrazolium dye (MTT) colorimetric assay for cellular growth and viability. *Methods Mol. Biol.* **716**, 157–168 (2011).
43. Swanson, K. et al. ADMET-AI: A machine learning ADMET platform for evaluation of large-scale chemical libraries. *Bioinformatics* **40**, btae16 (2024).
44. Banerjee, P., Kemmler, E., Dunkel, M. & Preissner, R. ProTox 3.0: A webserver for the prediction of toxicity of chemicals. *Nucleic Acids Res.* **52**, W513–W520 (2024).
45. Souers, A. J. et al. ABT-199, a potent and selective BCL-2 inhibitor, achieves antitumor activity while sparing platelets. *Nat. Med.* **19**, 202–208 (2013).
46. Birkinshaw, R. W. et al. Structures of BCL-2 in complex with venetoclax reveal the molecular basis of resistance mutations. *Nat. Commun.* **10**, 2385 (2019).
47. Oltersdorf, T. et al. An inhibitor of Bcl-2 family proteins induces regression of solid tumours. *Nature* **435**, 677–681 (2005).
48. Lee, E. F. et al. Crystal structure of ABT-737 complexed with Bcl-xL: Implications for selectivity of antagonists of the Bcl-2 family. *Cell Death Differ* **14**, 1711–1713 (2007).
49. Hargreaves, D. et al. Design of rigid protein–protein interaction inhibitors enables targeting of undruggable Mcl-1. *Proc. Natl. Acad. Sci.* **120**, e2221967120 (2023).
50. Hassaan, E., Eriksson, P.-O., Geschwindner, S., Heine, A. & Klebe, G. Fragments as novel starting points for tRNA-guanine transglycosylase inhibitors found by alternative screening strategies. *ChemMedChem* **15**, 324–337 (2020).
51. Koes, D. R., Baumgartner, M. P. & Camacho, C. J. Lessons learned in empirical scoring with smina from the CSAR 2011 benchmarking exercise. *J. Chem. Inf. Model.* **53**, 1893–1904 (2013).
52. Ostrowska, K. et al. Anticancer effects of O-aminoalkyl derivatives of alloxanthoxyletin and seselin. *Biomed. Pharmacother.* **95**, 1412–1424 (2017).
53. Jóźwiak, M. et al. Synthesis, structural studies and biological evaluation of connections of thiosemicarbazide, 1,2,4-triazole and 1,3,4-thiadiazole with palmitic acid. *Molecules* **23**, 822 (2018).

Acknowledgements

Computations were performed thanks to the Laboratory of Bioinformatics and Computational Genomics, Faculty of Mathematics and Information Science, Warsaw University of Technology using the Artificial Intelligence HPC platform financed by the Polish Ministry of Science and Higher Education (decision no. 7054/IA/SP/2020 of 2020-08-28).

Author contributions

W.O.: Manuscript review and editing, Anticancer studies, Supervision. K.S.: Cytotoxicity studies, data interpretation. P.R.: NMR experiment, Data interpretation. A.B.: Substrate synthesis, Data interpretation, Manuscript review and editing M.W.: In silico studies, Molecular docking. M.S.: Founding, Supervision. D.S.: Conceptualization, Tetrazole synthesis, Data collection and interpretation, Original manuscript writing, Supervision.

Funding

This work was supported by the internal grant of the Polish National Science Centre (2020/37/B/NZ2/03757).

Declarations

Competing interests

The authors declare no competing interests.

Additional information

Supplementary Information The online version contains supplementary material available at https://doi.org/10.1038/s41598-025-02781-7.

Correspondence and requests for materials should be addressed to D.S.

Reprints and permissions information is available at www.nature.com/reprints.

Publisher's note Springer Nature remains neutral with regard to jurisdictional claims in published maps and institutional affiliations.